Investigation of Electron Transport in a Cylindrical Hall Thruster using a Kinetic Code

Lubos Brieda*, Michael Keidar†
The George Washington University, Washington, D.C. 20052
Yevgeny Raitses‡ and Nathaniel J. Fisch§
Princeton University Plasma Physics Laboratory, Princeton, NJ 08543

In this paper, we investigate electron transport in the Princeton Cylindrical Hall thruster using a newly developed kinetic code. The code was coupled with the hybrid code HPHall, which was used to obtain initial values of ion and neutral densities, as well as the normal component of electric field. Our analysis was limited to a single magnetic field line, however, we considered the effect of varying surface roughness and magnetic field gradient on transport. Simulation results indicate strong influence of near-wall conductivity on total cross-field current. The anode current predicted by simulation was 0.09A.

I. Introduction

A well-documented anomaly observed in Hall thrusters is that electron current reaching the anode is significantly larger than what is predicted by classical models. This "anomalous" diffusion has several important implications. First, the anode current is directly related to the overall efficiency of the thruster. Electrons that escape the magnetic confinement do not ionize the working gas, and thus reduce the ionization efficiency. Understanding of the processes leading to the electron diffusion is necessary in order to optimize performance of these devices. Secondly, distribution of electrons influences the structure of plasma potential inside the device. Improvements in predictive modeling capability of Hall thrusters , needed in order to investigate phenomena such as lifetime or thruster performance, directly depend on our ability to compute the electron distribution.

The classical diffusion model states that cross-field transport is due to electrons colliding with ions and neutrals as they orbit around the field line. However, the close proximity of walls inside the Hall thruster leads to an additional transfer mechanism due to inelastic wall interactions. Surface impacts also result in emission of secondary electrons (SEE). Secondary electrons act to cool the main population,[1] since their initial temperature corresponds to that of the wall. However, of higher importance is their direct role on transport. If the initial velocity of SEE is arbitrary (as was the case in our analysis), , the magnetic field line orbited by the SEE will differ from that of the impacting electrons. As such, SEE directly contributes to transport. Collectively, these effects are known as *near-wall conductivity*.

In order to investigate the role of NWC on tranport, we have constructed a simulation code which directly resolved the orbital motion of electrons along a magnetic field line. This direct approach allowed us to obtain the radial variation in transport directly from the shifts of particle guiding centers. Our simulation domain consisted of a single magnetic field line bounded by dielectric walls. Only electrons were simulated. Sheath drop was computed self-consistently from the Poisson equation. This approach was similar to that of Sydorenko,[1] with the notable exception that we have taken into account the spatial variation of magnetic field.

We applied the code to the 2.6 cm Princeton cylindrical Hall thruster (CHT). This device, which is characterized in detail in Ref. 2, consists of a short annular anode region and a longer cylindrical acceleration

*PhD Candidate, Department of Mechanical and Aerospace Engineering, Member AIAA, lbrieda@gwu.edu
†Assistant Professor, Department of Mechanical and Aerospace Engineering, Associate Fellow, keidar@gwu.edu
‡Member AIAA
§Member AIAA

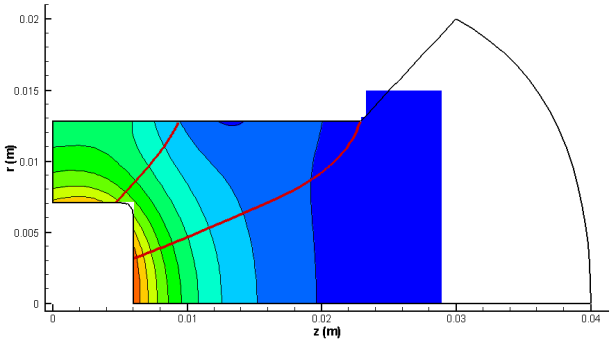

Figure 1. Plot of the computational domain. Two representative field lines are shown by thick black line. We considered the right-most line in the kinetic simulation. The black boundary corresponds to the domain used by HPHall. Contours show the magnitude of the magnetic field.

zone. The channel walls are made of Boron Nitride and Xenon is used as the working gas. The measured discharge current for the configuration studied in this paper was approximately 0.3 A. The device geometry leads to an interesting field configuration not seen in the traditional annular Hall thrusters. The convergence of field lines near the upstream end of the cylindrical region results in a magnetic field gradient. The mirroring effect is expected to reduce the flux of electrons to this wall. The strength of the magnetic field is shown in Figure 1. This figure also illustrates the field line used in our analysis.

Since our code tracked only electrons, we needed a radial distribution of ions and atoms in order to compute plasma potential and to model collisions. Experimental measurements were not available at the required resolution. Hence, we utilized HPHall, a 2D axi-symmetric code for Hall thruster discharges, to model the plasma properties inside the thruster. The computed values of particle densities were used as inputs to the kinetic code. HPHall results were also used to compute the perpendicular component of electric field, $E_\perp$. HPHall is described in more detail in the following section.

II. Hall Thruster Simulation

HPHall is an axi-symmetric hybrid code developed by Fife[3] to investigate plasma properties of the SPT-70 thruster. Since then, the code has been applied to various thruster designs.[4–6] HPHall uses the particle-in-cell method for the heavy particles. Plasma is assumed to be quasi-neutral. Electrons are modeled as 1D fluid. The axial variation in potential is computed by solving conservation equations along the thruster centerline. Electron temperature is assumed to remain constant along each magnetic field line. Under this assumption, the radial variation in potential is given by the thermalized model, $\phi^* = \phi - \frac{kT_e}{e}\ln(n_e)$.

HPHall solves the fluid equations only between the anode and the cathode. The position of the cathode boundary is one of the parameters affecting the potential distribution inside the device.[6] In our work, we performed only a minimal optimization study of the simulation parameters. The cathode was placed at z=27 mm, and we used the measurements from Refs. 7 and 8. to specify potential, temperature and density at this boundary. The specified values were used in the simulation were $\phi = 128$V, $kT_e = 21.7$eV and $n_e = 6e17\text{m}^{-3}$. The coefficient for the anomalous Bohm diffusion was set to 0.8, following the work of Garrigues.[9] Thruster operating condition was 250V of discharge voltage and propellant flow rate of 0.4mg/s. Chamber back pressure was 9mPa (6.7×10^{-5} Torr).

The computed plasma density is shown in Figure 2(a). In our work, we assumed that $n_e = n_i$, and disregarded any difference between singly and doubly charged ion populations. Figure 2(b) shows the variation in properties of interest along the magnetic field line. Neutral density ranges from 9×10^{18} to 2×10^{19} m^{-3}. Ion density range is 8×10^{16} to 7×10^{17} m^{-3}. The strongest normal electric field is concentrated near the dialectric walls, reaching over $20,000$V/m. The magnitude of the field in the channel center is approximately ± 1000V/m.

Axial variation of plasma potential and plasma density is shown in Figure 3. These results are compared to the experimental measurements from Ref. 8. As can be seen, using the stock parameters, the code was able reproduce the plasma density measured in the laboratory. The agreement with the potential profile is however not as good. The code predicts a stronger gradient of potential drop near the anode than is

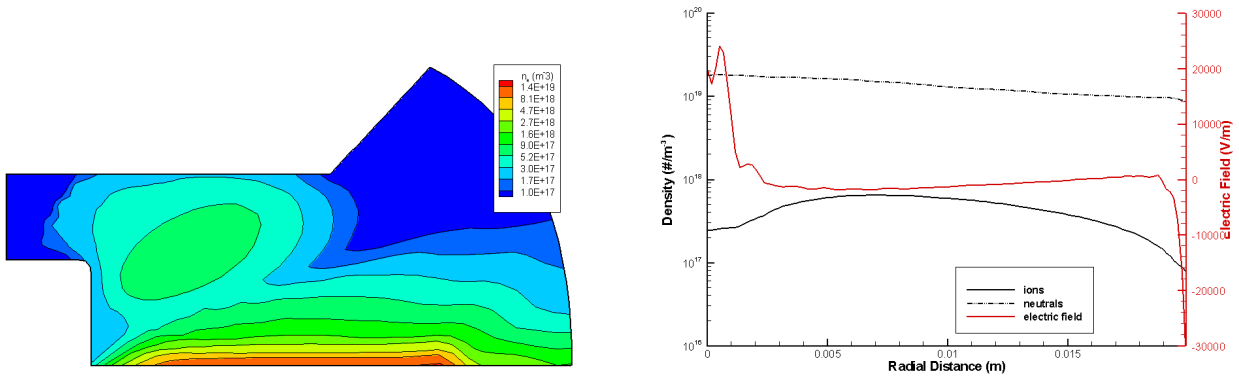

(a) Plasma Density (b) Cathode Line Properties

Figure 2. HPHall results showing computed values of plasma and neutral densities. Experimental data was used to specify cathode-line potential, density and temperature.

seen experimentally. This discrepancy will need to be addressed before the kinetic code can be used to directly predict the axial variation in mobility. However, in this paper we were primarily concerned with performing a parametric study of the transport behavior. The anode current predicted by HPHall was 0.008A, under-predicting the experimentally measured current by a factor of 37.

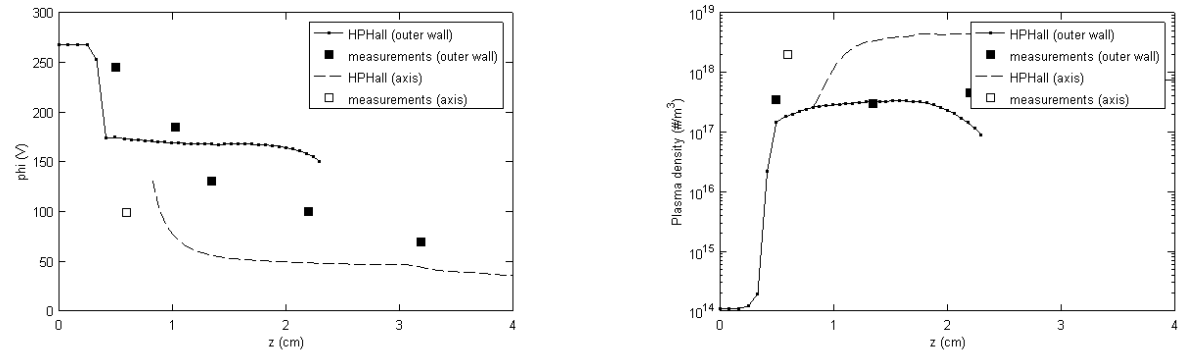

(a) Potential (b) Plasma Density

Figure 3. Comparison of HPHall results with experimental data. Experimental data from Ref. 8.

III. 1D Kinetic Code

A. Overview

The kinetic code used the particle-in-cell (PIC) method. Electrons were simulated as computational macro-particles. All three components of velocity and position were retained, however, plasma parameters varied only in one-dimension along the field line. Acceleration given by the Lorentz force, $F = q(\vec{E} + \vec{u} \times \vec{B}$ was integrated using the 4-step Boris method. Particle position were computed using the Leapfrog method. This method was chosen over Runge-Kutta method, as it provided comparable accuracy at fraction of the computational overhead. The initial distribution of electrons was determined from ion density. We first attempted to load electrons such that quasi-neutrality was retained at every simulation node. However, this approach led to an unstable sheath. Thus, the loading approach was modified such that at each node, electron charge corresponding to 0.99 of the ion charge was loaded. This charge reduction was analogous to prescribing an analytical electron density decay over some pre-defined sheath region. However, instead of specifying the sheath thickness as an input, we allowed the simulation to resolve the sheath self-consistently.

Electrons were loaded with a random tangential and normal velocity component corresponding to $kT_e = 15$ eV. This temperature corresponded to the electron temperature at the studied magnetic field line, as given by HPHall. At each time step, plasma potential was computed along the field line by a direct Poisson solver. Both ends of the computational domain were fixed at $\phi = 0$V. Electric field was obtained from $E_{\|} = -\partial\phi/\partial r$. Plot of a characteristic potential profile is shown in Figure 4. This figure also shows a typical velocity distribution profile at the end of the simulation. It should be noted that the potential solution develops initial oscillations, which are due to the finite particle loading. This effect is also demonstrated by the noise in the density data. We attempted to reduce these oscillations by increasing the number of computational particles and reducing the simulation time step. Simple smoothing operator was also implemented. Furthermore, to prevent this initial transient state from influencing the transport calculations, we initiated particle transport calculations only once the potential solution reached a steady behavior.

Since we were interested in resolving the non-neutral sheath, we set the cell size as $\Delta r = 0.5\lambda_D$. Number of simulation cells was 1120. Time step was set by considering orbital and translational motion of electrons. The time step used in the simulation was 1.4×10^{-12}s. At this temporal resolution, an electron completed a cyclotron orbit every 180 steps. Electron oscillations were resolved, and electrons took about 14 time steps to traverse through a cell. Simulation consisted of approximately 250,000 particles (2500 particles per cell). Total of 200,000 time steps was simulated. The simulation was performed serially using the 1048-node Sun X2200 M2 Pyramid cluster at The George Washington University.[10] Each case took approximately 6 hours to complete.

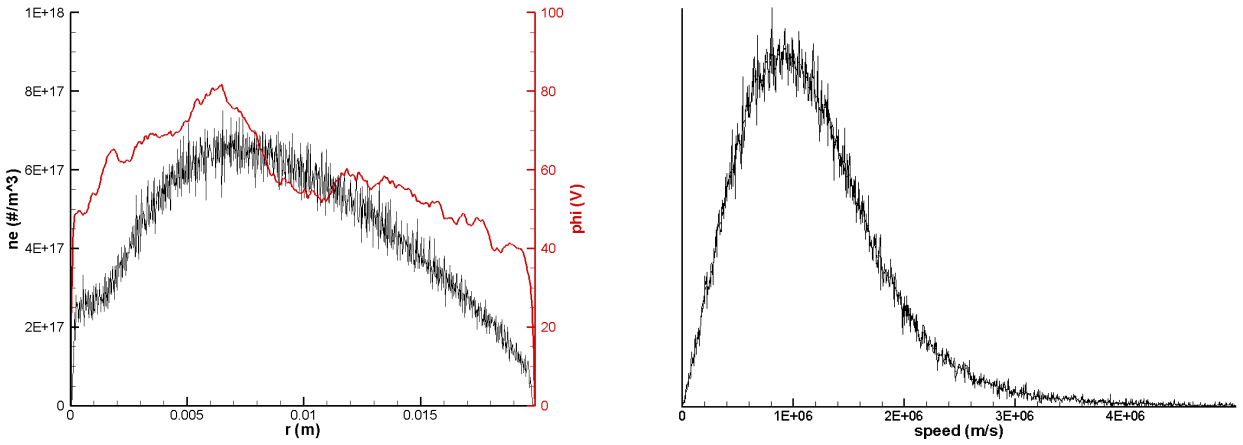

(a) Potential and Electron Density

(b) Distribution Function

Figure 4. Plot of typical simulation results, showing the variation in plasma potential, electron density, and the speed distribution function.

B. Collisions

Electron collisions were modeled using the Monte Carlo method. In this method, source particles are collided with a stationary target cloud. The collision probability is determined from background density, n_0 and collision frequency as $P = 1 - \exp(-n_0\sigma_0 g\Delta t)$. Here σ_0 is the total collision cross-section due to all processes. For particles undergoing collision, the collision process was picked randomly according to the ratio of σ_i/σ_0. Post-collision velocity was computed by first sampling a random target velocity and a random impact angle. We then calculated the post-collision velocity from conservation of energy.

Collision frequency is several orders of magnitude lower than the cyclotron frequency. In order to reduce numerical errors, collisions were performed only once per orbit. Two types of collisions were considered: electron-atom, and electron-ion. At low electron temperatures, polarization collisions are the dominant interaction process between electrons and neutral atoms.[11] Cross-section for this process was given by

$$\sigma_{Xe} = \left(\frac{\phi\alpha_p q^2}{\epsilon_0 m}\right)^{1/2} \frac{1}{v} \tag{1}$$

where α_r is the polarizability of the atom. It is given by $\alpha_r = 27.66a_0^3$, where a_0 is the Bohr radius.[12] Cross-section for electron-ion collisions was given by

$$\sigma_{Xe^+} = \frac{8}{\pi} b_0^2 \ln \Lambda \tag{2}$$

where $b_0 = q_1 q_2/(2\pi\epsilon_0 m v^2)$ is the distance of closest approach. The collision process was implemented by replacing the direction by a randomly sampled vector. Inelastic collision processes, such as ionization or excitation, were not included in our analysis.

C. Wall Effects

Electrons impacting the dielectric walls were reflected back into the simulation domain. No thermal accommodation was performed. However, in order to analyze the effect of surface roughness on transport, we implemented a roughness parameter k_s, which specified the probability a particle will be scattered by the wall. This parameter was varied from 0 (perfectly smooth surface) to 0.5 (half of impacting particles will diffuse). Scattered particles were reflected into the simulation domain by sampling a random velocity vector.

Electron impact also contributes to emission of secondary electrons (SEE) from the wall. The yield scales with the energy of the impacting particles, E_p. We used the linear fit of experimental measurements as given by Dunaevsky,[13]

$$\gamma = \left(\frac{E_p}{35\text{eV}}\right)^{0.5} \tag{3}$$

The SEE yield is non-negligible for $kTe = 15$eV. The SEE electrons were assumed to come off the surface unmagnetized, and were generated at the wall with initial direction given by a random velocity vector. In order to retain charge neutrality, impacting electrons were absorbed by the wall and were removed from the simulation.

D. Drifts

The crossed E and B configuration yields to drift of electrons in the direction perpendicular to both fields. In a Hall thruster, this $E \times B$ drift is oriented in the azimuthal direction, and hence does not contribute to anode current. Similar azimuthal drifts arise from curvature and gradient of the magnetic fields. However, due to the geometry of the cylindrical Hall thruster, the magnetic field develops a strong gradient in the tangential direction. This effect can be seen from the plot magnetic field magnitude, with the maximum effect observed near the upstream end of the cylindrical region. Conservation of magnetic moment dictates that perpendicular velocity of electrons must increase as the particles move to the region of stronger magnetic field. This in turn has the effect of reducing the tangential velocity in order to conserve particle's energy. The field line considered in this work intersects this region. As such, we expect reduced wall interaction near the center-pole due to the magnetic mirror effect. The tangential force acting on a particle as it travels into a region of increasing magnetic strength was given by

$$F_z = \frac{m v_\perp^2}{2B_z} \frac{\partial B_z}{\partial z} \tag{4}$$

E. Transport Calculation

We utilized two methods to characterize electron transport. First, we computed the spatial variation in current from shifts of particle guiding centers. The criteria for a particle leaving the field line was that its guiding center had shifted by a distance greater than the local Larmor radius. The guiding center was computed as the average of the minimum and maximum x position of the particle during the orbit, $x_g = 0.5(x^+ + x^-)$. Larmor radius was computed directly from the final tangential velocity. Only particles traveling towards the anode ($x_g < 0$) were considered. The diffused particles were removed from the simulation, and new particles were sampled at the radial position of the original particle. Total current was calculated by integrating the linear current density over the annular area swept by the field line.

We also computed the average drift velocity, $v_d = \bar{u}$. Mobility was then computed as $\mu = v_d/\bar{E}_\perp$. Here $\bar{E}_\perp$ is the average perpendicular component of the electric field. This method was not used to characterize the spatial variation in mobility due to a significant noise-to-data ratio and presence of regions with low

or near-zero $E_\perp$. The average drift velocity was computed by collecting the x-component of velocity for particles at each velocity integration step. Finally, in order to reduce errors due to statistical sampling, we ran a case in which all sources of transport were switched off. The resulting transport and drift velocity were assumed to be the baseline, and were subtracted from the subsequent runs.

F. Code Validation

The code was validated through a set of unit-tests. Particle integrator was tested by verifying energy conservation by integrating velocity of a particle for one million time steps. Potential solver was tested by using charge density variation with a known analytical solution. Collision frequency was compared with theory based on mean particle velocity and mean gas densities. Collisions were also used to characterize the transport algorithm. In this test, we loaded uniform ion density, $n_i = 10^{18}$ m^{-3}. Neutral density was zero. Collisions were represented by the hard-sphere model, $\sigma = 10^{-18}$ m^2. Electrons were loaded with $v_\perp = 10^6$m/s. Constant $E_\perp = 10,000$ V/m and $B_\parallel = 0.01$ T were also applied. Potential solver, SEE, and surface scatter were disabled. Collision frequency is $\nu = \tau^{-1} = n_i \sigma \bar{v} = 10^6$ Hz. Cyclotron frequency is $\omega_c = |q|B/m = 1.8 \times 10^9$ Hz. Mobility in the absence of magnetic confinement is defined as $\mu = |q|/m_e\nu = 1.8 \times 10^5$ T^{-1}. The cross-field mobility is then given as

$$\mu_\perp = \frac{\mu}{1 + \omega_c^2 \tau^2} \tag{5}$$

or $\mu_\perp = 0.057$ T^{-1}. Next, the drift velocity was computed, $v_d = \mu_\perp E_\perp = 568$m/s. Current is then given by $I = n_i q v_d A$, where A is the area swept by the field line. The theoretical value for the given inputs is $I = 0.15A$. The kinetic code predicted $I = 0.361A$. The two values agree within an order of magnitude. Drift velocity was calculated as $v_d = 69$m/s, under-predicting theory by an order of magnitude. Source of this discrepancy remains to be investigated.

IV. Results

We started the analysis by investigating the effect of surface roughness on electron diffusion. Profile of transport versus tangential distance along the field line is shown in Figure 5(a). The y axis in this plot corresponds to the total charge of particles moving towards the anode divided by the total simulation time. Total current was calculated by numerically integrating this linear current over the area swept by the field line, and dividing by the annular area. The integrated current for the five cases is shown in Figure 5(b).

Transport is concentrated in three distinct regions: zone near the center-pole, channel-zone dominated by collisions, and a narrow band due to SEE near the outer wall. We also observe that surface roughness plays only a minor role in diffusion. This observation can be explained by considering the yield of secondary electron, γ. At $kTe = 15eV$, γ exceeds all three studied values of surface roughness. Since the secondary electrons were assumed to be initially unmagnetized, they directly contributed to transport. This transport is demonstrated in the results as the narrow band near the outer wall. The configuration labeled *0.2, NC* shows transport in the absence of collisions. Total current decreased approximately by a factor of 2.5. This result illustrates the importance of wall collisions in Hall thrusters. Our model suggests that the cross-field transport is almost equally divided between effects due to particle collisions and electron-wall interactions.

We further investigated the influence of magnetic mirror on transport. Result labeled *0.2, NMG* shows results for a case identical to $k_s = 0.2$, with the exception that the $\partial B/\partial z$ term was set to zero. Total current for this configuration was not changed, however, the radial variation in transport was affected. While the previously analyzed cases showed no clear SEE influence near $r = 0$, this case demonstrates a clear SEE population in this region. To remind the reader, this region corresponds to the upstream end of the cylindrical zone, in which the magnetic field gradient reduces the flux of electrons reaching the wall. The reduction in collisional-transport is likely due to a change in electron tangential velocities, however, this observation remains to be investigated in more detail.

The predicted current was approximately 0.09A. Although this result shows an improvement over the predictions computed by HPHall, the experimental current is under-predicted by a factor of 3. Furthermore, as indicated in the previous section, our code over-estimated current for the simplified unit test by a factor of 2. This discrepancy corresponds to the 'anamalous' term not captured by our simulation. Additional work, taking into account inelestic collisions, as well as field osciallations, is clearly needed in order to improve the

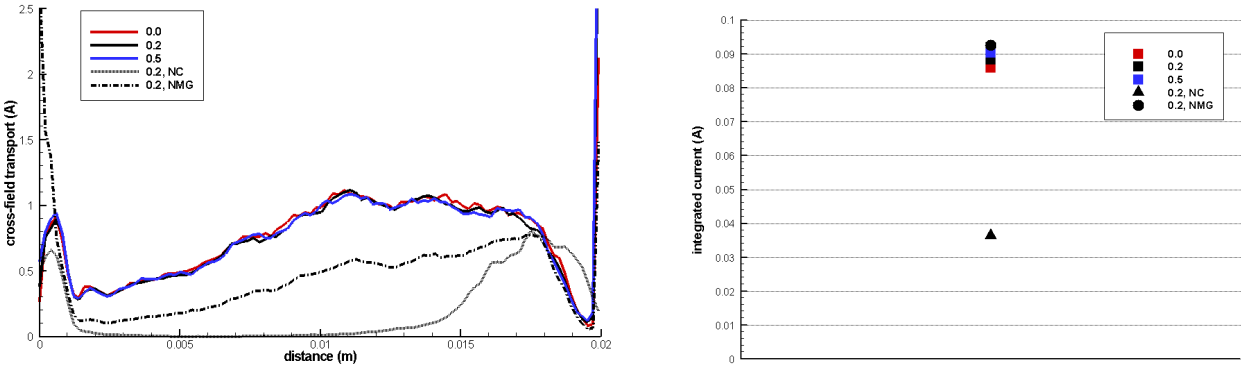

(a) Transport (b) Integrated Current

Figure 5. Simulation results, showing the spatial variation in transport, and the total integrated cross-field current, for three values of surface roughness. Transport in the absence of collisions in given by dataset *NC*. Dataset *NMG* corresponds to case in which the magnetic gradient was ignored.

agreement. We estimated the magnitude of the anamalous coefficent using the definition of Bohm mobility used in HPHall. Cross-field mobility in HPHall is defined as

$$\mu_\perp = \frac{\nu_m}{q + \omega_c^2 \tau^2} + K_B \frac{1}{16B} \tag{6}$$

where the first term on the RHS corresponds to the classical diffusion. K_B is the anomalous Bohm diffusion coefficient. Using the average values of B, $E_\perp$ and n_e of 0.3T, 860 V/m and 4.1×10^{17} m^{-3}, respectively, we obtain $v_d = 2,785$ m/s and $\mu_{\perp,x} = 3.2$ T^{-1}. Here we added the subscript $_x$ to indicate the experimental value. It should be noted that this estimated value of drift velocity agrees well with the value computed by the simulation. For $k_s = 0.2$, the code predicted $v_d = 3,256$ m/s. However, as mentioned in the previous section, this method did not pass our validation test and as such was not used in the current calculations. Mobility obtained by the kinetic code is $\mu_{\perp,s} = 0.97$ T^{-1}. Using this value in place of the classical model in Eq. 6, we obtain $K_b = 10.7$. It should be noted that this discrepancy is likely at least partly due to the poor agreement of potential profile (and hence $E_\perp$) from HPHall to the experimental data.

V. Conclusion

In this paper we used a kinetic code to investigate transport in the Princeton cylindrical Hall thruster. Our code predicted anode current in a reasonable agreement with the experimental measurements. Results indicate that near wall conductivity plays an important role in electron transport. Transport due to secondary electron emission was concentrated on the outer wall due to the strong magnetic mirroring effect near the upstream end of the cylindrical zone. We used the calculated mobility to estimate the anamalous diffusion coefficient. Source of this anomaly remains to be investigated. Future work will include detailed optimization of HPHall input parameters and coupling of calculated Bohm mobility with HPHall.

VI. Acknowledgments

The authors would like to thank Dr. Justin Koo at the Air Force Research Laboratory for valuable discussion and assistance in constructing the HPHall mesh.

References

[1]Sydorenko, D., Smolyakov, A., Kaganovich, I., and Raitses, Y., "Modification of Electron Velocity Distribution in Bounded Plasmas by Secondary Electron Emission," *IEEE Transactions on Plasma Science*, Vol. 34, No. 3, 2006, pp. 815–824.

[2]Smirnov, A., Raitses, Y., and Fisch, N., "Parametric investigation of miniaturized cylindrical and annular Hall thrusters," *Journal of Applied Physics*, Vol. 92, 2002, pp. 5673.

[3]Fife, J. M., *Hybrid-PIC Modeling and Electrostatic Probe Survey of Hall Thrusters*, Ph.D. thesis, Massachusetts Institute of Technology, Cambridge, MA, 1998.

[4]Hofer, R., Mikellides, I., Katz, I., and Goebel, D., "BPT-4000 Hall Thruster Discharge Chamber Erosion Model Comparison with Qualification Life Test Data," *30th International Electric Propulsion Conference*, 2007, pp. 2007–267.

[5]Ahedo, E., Maqueda, I., Antón, A., Raitses, Y., and Fisch, N., "Numerical simulations of a 2kW Hall thruster," *42th Joint Propulsion Conference, Sacramento, CA*, 2006, pp. 2006–4655.

[6]Nakles, M., Hargus, W., and VanGilder, D., "Comparison of Numerical and Experimental Near-Field Ion Velocity Distributions of the BHT-200-X3 Hall Thruster," *42nd Joint Propulsion Conference, Sacramento, CA*, 2006, AIAA-2006-4479.

[7]Raitses, Y., Smirnov, A., and Fisch, N., "Effects of enhanced cathode electron emission on Hall thruster operation," *Physics of Plasmas*, Vol. 16, 2009, pp. 057106.

[8]Smirnov, A., Raitses, Y., and Fisch, N. J., "Plasma measurements in a 100W cylindrical Hall thruster," *Journal of Applied Physics*, Vol. 95, No. 5, 2004, pp. 2283–2291.

[9]Garrigues, L., Hagelaar, G. J. M., Boeuf, J. P., Raitses, Y., Smirnov, A., and Fisch, N. J., "Two Dimensional Hybrid Model of a Miniaturized Cylindrical Hall Thruster," *30^{th} International Electric Propulsion Conference*, Florence, Italy, 2007, IEPC-2007-157.

[10]"Institute for Massively Parallel Applications and Computing Technologies," http://hpcl.seas.gwu.edu/impact/.

[11]Lieberman, M. and Lichtenberg, A., *Principles of plasma discharges and materials processing*, Wiley-interscience, 2005.

[12]Nicklass, A., Dolg, M., Stoll, H., and Preuss, H., "Ab initio energy-adjusted pseudopotentials for the noble gases Ne through Xe: Calculation of atomic dipole and quadrupole polarizabilities," *Journal of Chemical Physics*, 1995.

[13]Dunaevsky, A., Raitses, Y., and Fisch, N., "Secondary electron emission from dielectric materials of a Hall thruster with segmented electrodes," *Physics of Plasmas*, Vol. 10, 2003, pp. 2574.